

Relative phase-dependent two-electron emission dynamics with two-color circularly polarized laser fields

Tong-Tong Xu(徐彤彤), Lian-Lian Zhang(张莲莲), Zhao Jin(金钊), Wei-Jiang Gong(公卫江)

Citation: Chin. Phys. B . 2020, 29(9): 093202 . **doi:** 10.1088/1674-1056/ab928c
Journal homepage: http://cpb.iphy.ac.cn; http://iopscience.iop.org/cpb

What follows is a list of articles you may be interested in

Multiphoton quantum dynamics of many-electron atomic and molecular systems in intense laser fields

Peng-Cheng Li(李鹏程), Shih-I Chu

Chin. Phys. B . 2020, 29(8): 083202 . **doi:** 10.1088/1674-1056/ab9c0f

Controlling electron collision by counterrotating circular two-color laser fields

Baoqin Li(李宝琴), Xianghe Ren(任向河), Jingtao Zhang(张敬涛)

Chin. Phys. B . 2020, 29(4): 043202 . **doi:** 10.1088/1674-1056/ab7907

Relative phase effect of nonsequential double ionization in Ar by two-color elliptically polarized laser field

Jia-He Chen(陈佳贺), Tong-Tong Xu(徐彤彤), Tao Han(韩涛), Yue Sun(孙悦), Qing-Yun Xu(徐清芸), Xue-Shen Liu(刘学深)

Chin. Phys. B . 2020, 29(1): 013203 . **doi:** 10.1088/1674-1056/ab5d03

Effect of elliptical polarizations on nonsequential double ionization in two-color elliptically polarized laser fields

Tong-Tong Xu(徐彤彤), Jia-He Chen(陈佳贺), Xue-Fei Pan(潘雪飞), Hong-Dan Zhang(张宏丹), Shuai Ben(贲帅), Xue-Shen Liu(刘学深)

Chin. Phys. B . 2018, 27(9): 093201 . **doi:** 10.1088/1674-1056/27/9/093201

Electron correlations in nonsequential double ionization of argon atoms by elliptically polarized laser pulses

Yu Ben-Hai, Li Ying-Bin, Tang Qing-Bin

Chin. Phys. B . 2013, 22(1): 013206 . **doi:** 10.1088/1674-1056/22/1/013206

Relative phase-dependent two-electron emission dynamics with two-color circularly polarized laser fields*

Tong-Tong Xu(徐彤彤)†, Lian-Lian Zhang(张莲莲), Zhao Jin(金钊), and Wei-Jiang Gong(公卫江)

College of Sciences, Northeastern University, Shenyang 110819, *China*

(Received 31 March 2020; revised manuscript received 28 April 2020; accepted manuscript online 13 May 2020)

With the semiclassical ensemble model, we explore the relative phase-dependent nonsequential double ionization (NSDI) of Mg by counter-rotating two-color circularly polarized (TCCP) laser pulses. The yield of Mg^{2+} sensitively depends on the relative phase $\Delta\varphi$ and the intensity of TCCP laser fields. At $\Delta\varphi = 1.5\pi$, the yield of Mg^{2+} exhibits a pronounced peak in the 0.05 PW/cm^2 laser field. This behavior results from the increase of the initial transverse velocity compensating for the drift velocity with the decreasing angle by analyzing the angular distributions of the electron pairs in four relative phases. By changing the relative phases, we find that the recollision excitation with subsequent ionization and the recollision-impact ionization mechanisms can be controlled with TCCP laser fields.

Keywords: nonsequential double ionization, relative phases, two-electron emission dynamics

PACS: 32.80.Rm, 42.50.Hz, 42.65.Ky **DOI:** 10.1088/1674-1056/ab928c

1. Introduction

Nonsequential double ionization (NSDI) of atoms in intense laser fields gains extensive attention, due to the first observation of the knee structure on the yield of Xe^{2+} as a function of the laser intensity.[1] The mechanism of NSDI has been a hot topic for nearly four decades.[2–4] Despite the rapid progress on NSDI, many theoretical studies and experimental phenomena still constantly appear and overturn our current knowledge. Recent cases include timing the release of the correlated electrons in strong-field NSDI by counter-rotating two-color circularly polarized (TCCP) laser fields,[5] the double-triangle structure in the momentum distribution at high intensity,[6] and the double-ionization probability sensitive depending on the relative intensity in counter-rotating TCCP laser fields.[7]

In recent years, TCCP laser fields have attracted interests of the strong-field community due to their widespread applications, for instance, the generation of circularly polarized high-order harmonics (HHG),[8] driving high-order above-threshold ionization (HATI),[9,10] a spiral structure on the molecular photoelectron momentum distribution (PMD),[11] the enhancing electron recollision of N_2 molecules and Ar atoms by controlling the helicity and field ratio between the two colors,[12] and multiple recollision dynamics in NSDI.[13] In NSDI process, the electron–electron interaction exhibits highly correlated behavior and many studies have been carried out to present the microscopic dynamics of the electron–electron correlation in recent several decades.[14–24] Two ionization pathways exist in NSDI. One is the recollision excitation with subsequent ionization (RESI) and the other is the recollision-impact ionization (RII).[25]

During the study of controlling the electron–electron emission directions and correlation in the NSDI processes, most of the experimental observation and theoretical study have been carried out by changing the form of the lasers fields. For example, the asymmetry of the correlated momentum distribution for NSDI strongly depends on the carrier-envelope phase (CEP) in the near-single-cycle laser field.[26,27] Likewise, RESI and RII channels can be controlled by the variation of the CEPs in few-cycle elliptically polarized laser fields.[28] Also, for the yield of Ne^{2+}, the directions of electron–electron emission and the correlation are sensitively dependent on the relative phase in orthogonally polarized two-color (OTC) laser fields.[29,30]

Recently, a number of works about NSDI in counter-rotating TCCP laser fields have been reported.[7,31,32] The electron dynamics of NSDI in a laser field have been proposed and demonstrated both experimentally and theoretically.[33–35] Despite the great progress on dynamics of the correlated electrons in counter-rotating TCCP laser pulses, we note that no systematic theoretical study has been presented to demonstrate the dynamics in NSDI with different relative CEPs. Therefore, in this paper, we systematically study the relative phase-dependent NSDI of Mg with counter-rotating TCCP laser pulses. Furthermore, we focus on the yield of Mg^{2+} with different relative phases and the possibility of controlling over the RESI and RII. Our results show that the yield of Mg^{2+} sensitively depends on the relative phases $\Delta\varphi$ and the intensity of TCCP laser fields. By analyzing of the angular distributions of the emitting electrons with four relative phases, the initial

*Project supported by the China Postdoctoral Science Foundation (Grant No. 2019M661108) and the Fundamental Research Funds for the Central Universities, China (Grant No. N2005023).

†Corresponding author. E-mail: xutongtong@mail.neu.edu.cn

© 2020 Chinese Physical Society and IOP Publishing Ltd

transverse velocity compensating for the drift velocity can increase with the decreasing angle. This behavior leads to more tunneling electrons driven back to the parent ion and the increase of the yields of Mg^{2+}. The recollision time and energy are also investigated. Our results indicate that RESI and RII mechanisms can be controlled by the relative phases.

2. Theoretical model

Accurate demonstration of NSDI in strong laser fields needs full quantum theory. Nevertheless, a numerical solution of the time-dependent Schrödinger equation for multi-electron systems requires a huge computational condition.[22,36,37] For the last decade or more, a considerable amount of theoretical research works on NSDI have adopted the semiclassical and classical methods. It has been tested and confirmed that the two methods are very helpful not only in analyzing the results of the experiments[38–40] but also in forecasting all kinds of phenomena in single or double ionization.[41] In addition, the trajectory of every electron can be traced in the whole NSDI process with semiclassical and classical models and exhibits an intuitive picture.[24,30,42] Thus, we use the two-dimensional (2D) semiclassical ensemble model[36,37] to investigate two-electron emission dynamics of NSDI by counter-rotating TCCP laser pulses.

In the semiclassical model, an electron is released through quantum tunneling.[43] The transverse velocity of this electron satisfies Gaussian distribution and the parallel velocity of the tunneled electron (parallel to the transient electric field of the laser pulse) is zero.[44] The weight of each trajectory is evaluated by $w(t_0, v^i_{\perp 0}) = w(t_0)w(v^i_{\perp 0})$, in which

$$w(t_0) = \left(\frac{2(2I_{\rm p1})^{1/2}}{|\boldsymbol{E}(t_0)|}\right)^{\frac{2}{\sqrt{2I_{\rm p1}}}-1} \exp\left(\frac{-2(2I_{\rm p1})^{3/2}}{3|\boldsymbol{E}(t_0)|}\right), \quad (1)$$

$$w(v_{\perp 0}) = \frac{1}{|\boldsymbol{E}(t_0)|} \exp\left(-\frac{(v_{\perp 0})^2(2I_{\rm p1})^{1/2}}{|\boldsymbol{E}(t_0)|}\right). \quad (2)$$

Here $v_{\perp 0}$ is the initial transverse momentum, t_0 is the tunneling time and $\boldsymbol{E}(t_0)$ is the instantaneous electric field at t_0. The bound electron satisfies a microcanonical distribution.[45] After the electron is ionized through quantum tunneling, the subsequent evolution of the two electrons in the combined laser and Coulomb fields is governed by the classical Newtonian equation (atomic units are used throughout unless stated otherwise):

$$\frac{{\rm d}^2\boldsymbol{r}_i}{{\rm d}t^2} = -\nabla[V_{\rm ee}(\boldsymbol{r}_1, \boldsymbol{r}_2) + V_{\rm ne}(\boldsymbol{r}_i)] - \boldsymbol{E}(t), \quad (3)$$

where the subscript i is the labels of the ionized electrons, and $\boldsymbol{r}_1, \boldsymbol{r}_2$ are the coordinates of two electrons. $V_{\rm ee}(\boldsymbol{r}_1, \boldsymbol{r}_2) = (\boldsymbol{r}_1 - \boldsymbol{r}_2)^{-1}$ and $V_{\rm ne}(\boldsymbol{r}_i) = -2(\boldsymbol{r}_i^2 + a^2)^{-1/2}$ are the electron–electron and electron–ion interaction potentials, respectively. $I_{\rm p1} = 0.28$ a.u. and $I_{\rm p2} = 0.55$ a.u. are the ionization potentials, which match the first and second ionization potentials of magnesium atoms. We choose the soft parameter $a = 3.0$ to avoid autoionization.[46,47]

The counter-rotating TCCP laser field is written as $\boldsymbol{E}(t) = \boldsymbol{E}_{\rm r}(t) + \boldsymbol{E}_{\rm b}(t)$, where

$$\boldsymbol{E}_{\rm r}(t) = \frac{E_0}{(1+\gamma_{\rm E})} f(t)[\cos(\omega_{\rm r} t)\hat{x} + \sin(\omega_{\rm r} t)\hat{y}], \quad (4)$$

and

$$\boldsymbol{E}_{\rm b}(t) = \frac{\gamma_{\rm E} E_0}{(1+\gamma_{\rm E})} f(t)[\cos(\omega_{\rm b} t + \Delta\varphi)\hat{x} - \sin(\omega_{\rm b} t + \Delta\varphi)\hat{y}]. \quad (5)$$

Here $\omega_{\rm r} = 0.0576$ a.u. is the fundamental frequency and $\omega_{\rm b} = 0.112$ a.u. is the second harmonic frequency. E_0 is the maximum combined electric field amplitude, and $\gamma_{\rm E} = 2$ (the probability of rescattered electron is maximized)[31] is the electric field amplitude ratio between the two laser fields. $\Delta\varphi$ is the relative phase and $f(t)$ is the pulse envelope, which can be given by

$$f(t) = \begin{cases} 1, & t \le 3T_1, \\ \cos^2\left(\dfrac{(t-3T_1)\pi}{1.5T_1}\right), & 3T_1 < t \le 5T_1, \\ 0, & t > 5T_1. \end{cases} \quad (6)$$

In the above equation, T_1 is the optical period of the fundamental laser field $\boldsymbol{E}_{\rm r}(t)$.

In the calculations, 10^7 weighted classical electron trajectories are calculated from t_0 to the end of the laser field. For each $\Delta\varphi$, more than 10^5 double ionization events occur. The event is defined as double ionization when the energies of the two electrons are positive at the end of the laser pulses. We will not consider the nonadiabatic transitions and multiphoton transitions in our calculations. We focus on the correspondence between the relative phases and the angular of the electrons' final momentum (the ion momentum distribution, the yield of Mg^{2+}, the recollision energy, and the release time). The tunneling theory has no effect on qualitative results, thus we use the semiclassical model.

3. Results and discussion

Figure 1(a) shows the yields of Mg^{2+} as a function of the relative phase $\Delta\varphi$ at different intensities. The yield of Mg^{2+} sensitively depends on $\Delta\varphi$ and presents a outstanding peak at certain values of $\Delta\varphi$. For example, the yield of Mg^{2+} reaches a maximum around $\Delta\varphi = 1.5\pi$ for the laser intensity of 0.05 PW/cm^2. The peaks of yields are around $\Delta\varphi = 1.42\pi$ and $\Delta\varphi = 1.34\pi$ for the intensities of 0.07 PW/cm^2 and 0.09 PW/cm^2, respectively. The previous NSDI of Ne

atoms in OTC laser fields illustrated in Ref. [30] shows that the yields of Ne^{2+} depends on $\Delta\varphi$ and the maximal yield is around $\Delta\varphi = (n+0.5)\pi$, $n \in N$. Moreover, the yield of Mg^{2+} increases with larger field strength. These are similar to the results reported in Ref. [30]. The behavior is coined as trajectory concentration effect in OTC laser fields, while for TCCP laser fields, the yield of Mg^{2+} is relative to the angular distribution of the photoelectrons, as will be shown in the following.

To understand the relative phase dependence of the yield of Mg^{2+} mentioned above, we make statistics on the number of the trajectories that result in double ionization (DI). For the three intensities, the number of DI trajectories sensitively depends on the $\Delta\varphi$, as shown in Fig. 1(b). The yield of Mg^{2+} is relative to the corresponding weights given by tunnel ionization rate and their number of DI trajectories. The dependence of Mg^{2+} yield on $\Delta\varphi$ exhibits an similar trend as that for the number of DI trajectories, as shown in Fig. 1(a). Figure 1(c) shows the tunnel ionization rate versus the relative phase $\Delta\varphi$ at three intensities. The tunnel ionization rate varies with $\Delta\varphi$ and the peak of the distribution shifts to left slightly as the laser intensity increases. In addition, for the 0.09 PW/cm^2, the tunnel ionization rate varies relatively slowly as $\Delta\varphi$ changes, as shown in Fig. 1(c). This phenomenon indicates that the laser intensity is near the saturation regime.[29,30]

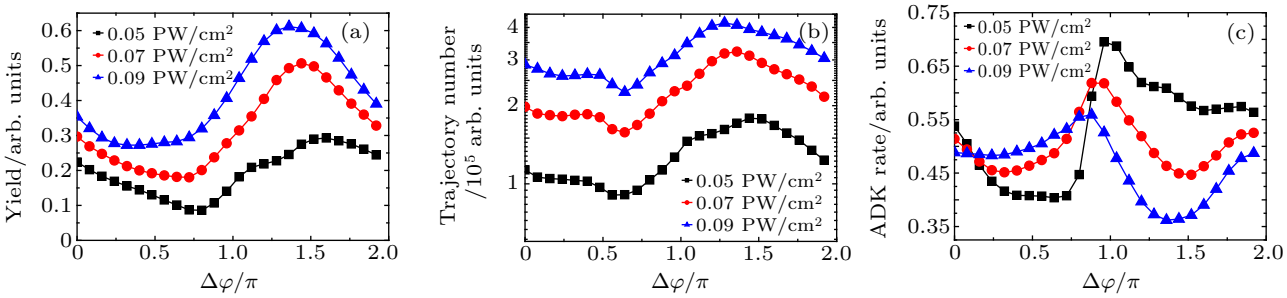


Fig. 1. (a) Yield of Mg^{2+}, (b) number of DI trajectories and (c) ionization rate of the tunneling electrons calculated with the ADK theory[43] versus the relative phase at intensities of 0.05 PW/cm^2 (black line with squares), 0.07 PW/cm^2 (red line with dots), and 0.09 PW/cm^2 (blue line with triangles).

To obtain more details about the transition behavior mentioned above and the two-electron correlated dynamics, the angular distribution of the photoelectrons is investigated. We take the case of 0.05 PW/cm^2 laser intensity as an example and analyze the angular distribution of the correlated two-electron. The angular distributions of electrons from the singly ionized (SI) events (black squares) and electrons from the NSDI events (red dots) are shown on the left of Fig. 2. For $\Delta\varphi = 0.6\pi$, the angles from the SI events are mainly distributed about 125°, as shown in Fig. 2(a). While the angular distributions of electrons from the SI events slightly change with the increase of the relative phases $\Delta\varphi$, i.e., the relative phase $\Delta\varphi = 0.8\pi$, $\Delta\varphi = 1.0\pi$, and $\Delta\varphi = 1.2\pi$, the angular distributions of the SI events are mainly distributed about 115°, 100°, and 85°, respectively [as shown in Figs. 2(b)–2(d)]. These distributions indicate the relative phase-dependence of the angular distributions from the SI events.

In circularly polarized (CP) laser fields, the classical method[48] reveals that the drift velocity of electron emission along the negative direction results in the electron leaving away from its parent ion without coming back. If the initial transverse velocity can compensate for the drift velocity, the recollision will occur.[40,49,50] For $\Delta\varphi = 0.6\pi$, the angle from the SI events is mainly distributed about 125° [black squares in Fig. 2(a)], the drift velocity can be compensated less by the initial transverse velocity than that for $\Delta\varphi = 0.8\pi$, $\Delta\varphi = 1.0\pi$, and $\Delta\varphi = 1.2\pi$ [as shown in Figs. 2(b)–2(c)], where the initial transverse velocity is the velocity component of the vertical direction at the time of ionization of the first electron. As the angles decrease (115°, 100°, and 85°), the initial transverse velocity compensating for the drift velocity will increase, which leads to more tunneling electrons driven back to the parent ion. Thus, the yield of the Mg^{2+} increases as the relative phase increases ($\Delta\varphi \in [0.6\pi,\ 1.5\pi]$), as shown in Fig. 1(a).

For the NSDI events, the angular momentum distributions of the electrons are also shown on the left of Fig. 2. In the SI events, the tunneling electron emits around the maximal laser field, thus we can perform the statistical analysis of the electron angular distribution of the SI events to mark the time. There is a shift between the distribution of the NSDI and SI with different relative phases as shown on the left of Fig. 2. There is the same phenomenon in the experimental observations,[7] the shift results from the increasing influence of the Coulomb potential for the distribution of NSDI events as compared to the SI events.

Using the semiclassical ensemble model, we can distinguish the two electrons in NSDI processes. In order to know details of correlated electron dynamics, the angular distributions of the bound and the recollision electrons are shown on the right of Fig. 2, where more details of the ionization dynamics could be inferred. For the case of $\Delta\varphi = 0.6\pi$, 0.8π, 1.0π, and 1.2π, there exists a slight angular change between the distribution for the SI (the black square) and recollision electrons (the red dot). For the recollision electron, the posi-

tions of the peak in the distribution slightly change from those of the SI events. For the bound electron (the blue triangle), however, the positions of these peeks are very near those of the SI events. The recollision electron is ionized through tunneling. Without recollision in NSDI events, the angular distributions of recollision and SI electrons should be the same. Thus, the change in the angular distributions of SI events and the recollision electron is caused by the recollision. However, the angular change is not too big. This indicates that collision is not too strong. Because of the soft recollision, the reollision electron transfers too little energy to collide out the other electron. If the bound electron is released by the RESI mechanism, it will be ionized around the maximum of the electric field. In consequence, the angular distribution of the bound electron is similar to that of the SI events. By analyzing the angular distribution, we can provide that the RESI path is prevalent in the $\gamma_E = 2$ laser fields for the case of $\Delta\varphi = 0.6\pi$, 0.8π, 1.0π, and 1.2π at the intensity of 0.05 PW/cm^2.

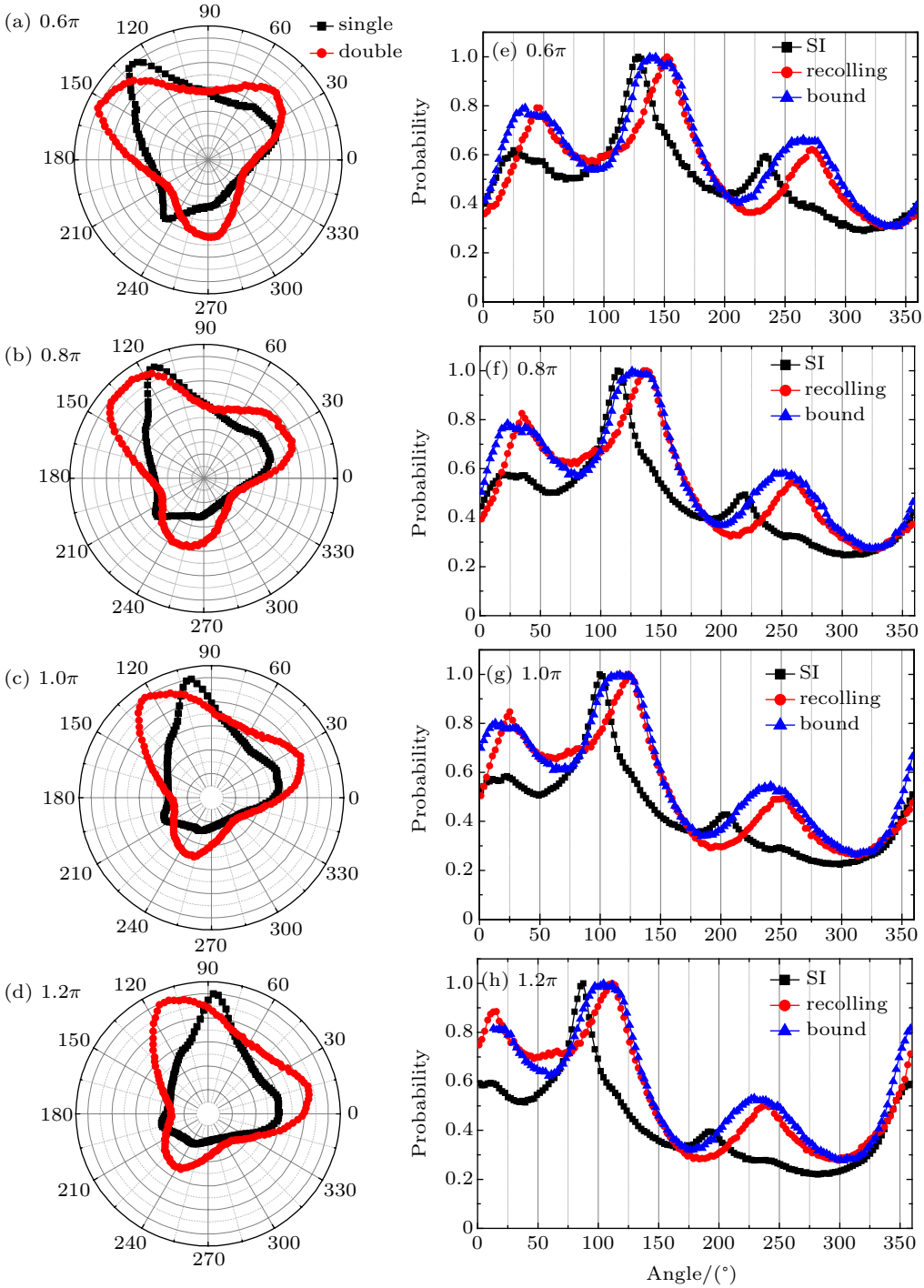


Fig. 2. The releasing angle distributions of the electrons for the SI (black squares) and the NSDI events (red dots) for the case of $\Delta\varphi = 0.6\pi$ (a), 0.8π (b), 1.0π (c), and 1.2π (d) in counter-rotating TCCP fields, respectively. The releasing angle distribution of the electrons for the SI events (black squares), the recolliding (red dots) and the bound electrons (blue triangles) in NSDI for the case of $\Delta\varphi = 0.6\pi$ (e), 0.8π (f), 1.0π (g), and 1.2π (h). The combined intensity of the laser field is 0.05 PW/cm^2.

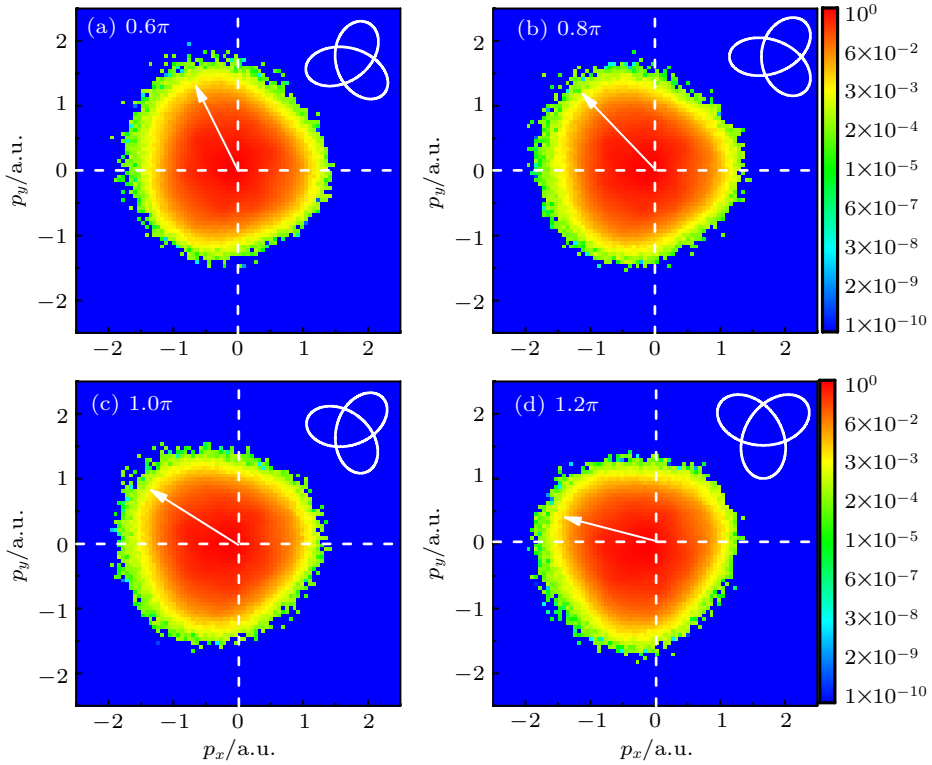


Fig. 3. The ion momentum distribution for the case of $\Delta\varphi = 0.6\pi$ (a), 0.8π (b), 1.0π (c), and 1.2π (d) with counter-rotating TCCP fields, respectively. The white line with arrow acts as guide to the eyes regarding the rotation of the ion momentum distribution. The insets in (a)–(d) show the Lissajous curves of the counter-rotating TCCP laser fields. The intensity of the laser field is 0.05 PW/cm^2.

To understand the electron correlation in NSDI, we present the ion momentum distribution for $\Delta\varphi = 0.6\pi$ (a), 0.8π (b), 1.0π (c), and 1.2π (d) in Fig. 3. The white line with arrow acts as guide to the eyes regarding the rotation of the ion momentum distribution. The electric fields of the counter-rotating TCCP (Lissajous curves) for the case of $\Delta\varphi = 0.6\pi$ (a), 0.8π (b), 1.0π (c), and 1.2π (d) are shown in the inset of Figs. 3(a)–3(d). We can clearly see that the Lissajous curves are rotated and present the special symmetries. Therefore, the ion momentum distribution presents a counterclockwise rotation and threefold structure symmetrically as shown in Figs. 3(a)–3(d). Furthermore, the ion momentum distribution can indicate the electron–electron correlation. The area of ion momentum distribution will be smaller if the two electrons are released to opposite directions than that if the two electrons are released in the same direction.[13,51] These ion momentums are mainly distributed near the origin, which indicates that anticorrelated behavior between the two electrons (RESI path) is prevalent at four different relative phases $\Delta\varphi$. This phenomenon demonstrated in Fig. 3 is in accordance with that illustrated on the left of Fig. 2. The releasing angle distributions of the electrons for the NSDI events (red dots) [as shown on the left of Fig. 2] mainly distribute about 150°, 135°, 130°, and 110°. This is similar to the results reported in Ref. [7].

Figure 4 shows the trajectory probability and the yield of RII and RESI as a function of the relative phases. Here we define RII (RESI) as the ionization mechanism, in which the interval between recollision time and double ionization time is less than 0.25 optical cycle (o.c.) (more than 0.25 o.c.). Figure 4(a) shows the trajectory probabilities of RII and RESI as a function of the relative phases $\Delta\varphi$. It is clearly seen that controlling the RII and RESI can be possible by changing relative phases. For $\Delta\varphi = 0.75\pi$ and $\Delta\varphi = 1.5\pi$, the paths of RII (RESI) could be turned on (off) and turned off (on), respectively. Figure 4(b) shows the yields of RII and RESI versus the relative phases $\Delta\varphi$. The yield is relative to the corresponding weights given by tunnel ionization rate and their number of RII and RESI trajectories, respectively. The paths of RII (RESI) could

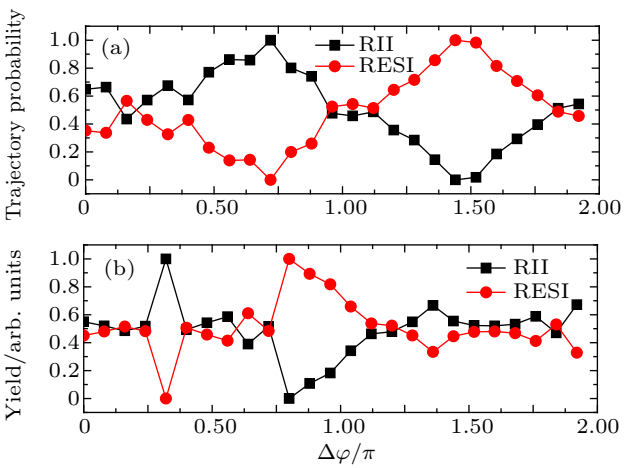


Fig. 4. (a) The trajectory probability, and (b) the yield of RII and RESI versus the relative phases $\Delta\varphi$ for the intensity of 0.5 PW/cm^2.

be turned on (off) and turned off (on) at $\Delta\varphi = 0.32\pi$ and $\Delta\varphi = 0.8\pi$, respectively. The positions of turning on (off) the RII and RESI paths between the trajectory probability and the yields are different. Thus, the weights given by tunnel ionization rate is significant effect on controlling the RII and RESI paths in the NSDI processes.

To gain insight into the relative phase-dependent of RII and RESI mechanisms, we trace the trajectories of recollision electron and show the probability distribution of the recollision energy ($E_r(t_r - \Delta t)$). It is defined as the energy of the recollision electron at the moment $\Delta t = 3$ a.u. before recollision t_r.[23] The probability distributions of the reocollision energy are mainly distributed around the small returning energy, as shown in Fig. 5. It also indicates that RESI paths are prevalent for four relative phases. However, the other peak of the recollision energy for $\Delta\varphi = 0.6\pi$ [the black line with squares in Fig. 5] is significantly higher than that for $\Delta\varphi = 0.8\pi$ [the red line with dots in Fig. 5]. Furthermore, the peaks of recollision energy shift to left as the relative phases increase. Thus, the events of soft recollision increase as the relative phases increase, i.e., the paths of the RESI increase with the increase of the relative phases ($\Delta\varphi \in [0.75\pi,\ 1.2\pi]$), which is in agreement with the trajectory probability illustrated in Fig. 4(a).

Finally, we trace the NSDI trajectories and show the probability of the recollision time for $\Delta\varphi = 0.6\pi$, 0.8π, 1.0π, and 1.2π in Fig. 6. The distribution of the recollision time spans over a wide range for the four relative phases $\Delta\varphi = 0.6\pi$, 0.8π, 1.0π, and 1.2π, as shown in Figs. 6(a)–6(d). The peak moves from the falling edge to the peak of the 800-nm laser pulse (blue solid curves). For ionization by OTC laser fields,[30] the peak of the probability moves near the peak of the electric field as the relative phases increase from $\Delta\varphi = 0.0\pi$ to $\Delta\varphi = 0.5\pi$. This phenomenon is the same in our counter-rotating TCCP laser fields. The recollision time for four relative phases are significantly different in Fig. 6. The peak of the recollision time in distribution moves to the maximal laser filed as the relative phase increases. This indicates that controlling the recollision time can be performed by changing the relative phases. The results mentioned above shows that the recollision energy and time are strongly dependent on the relative phases.

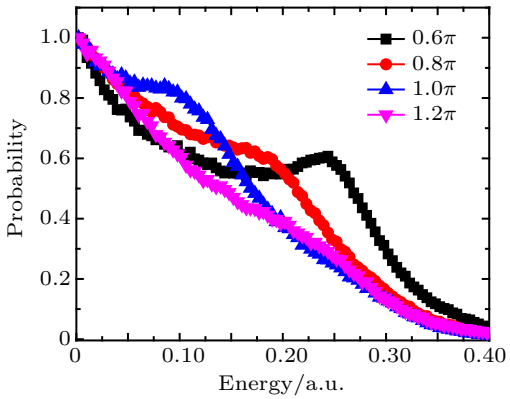


Fig. 5. The probability distribution of the recollision energy for the relative phases $\Delta\varphi = 0.6\pi$ (a), 0.8π (b), 1.0π (c), and 1.2π (d).

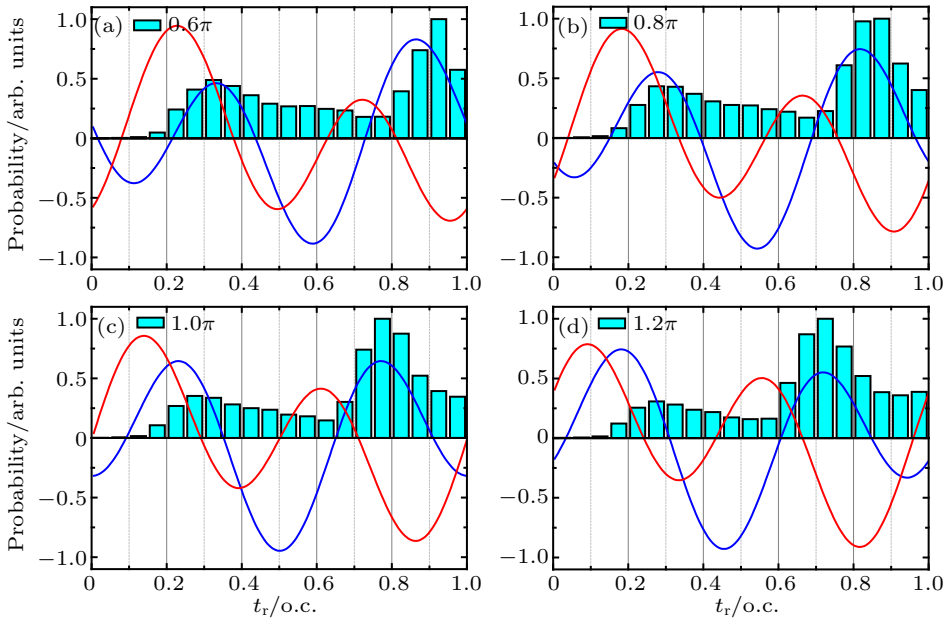


Fig. 6. Probability distribution of the recollision time for $\Delta\varphi = 0.6\pi$ (a), 0.8π (b), 1.0π (c), and 1.2π (d). The red and blue solid curves represent the 400-nm and 800-nm laser fields, respectively.

4. Conclusions

In summary, we have theoretically investigated the relative phase-dependent two-electron emission dynamics with counter-rotating TCCP laser fields. It is shown that the yield of Mg^{2+} sensitively depends on $\Delta\varphi$ and an outstanding peak appears at particular values of $\Delta\varphi$. The dynamical information about single, recollision and bound electrons could be obtained by analyzing the relative releasing angle of the two

electrons. Furthermore, the yield of Mg^{2+} increases with the decreasing angle. The ion momentum distributions for four relative phases are investigated. The counterclockwise rotation in distributions is caused by the relative phases. The RII and RESI could be controlled by the relative phases of the laser fields by analysis of the distribution of recollision energy. Our predictions can be helpful for the stimulating further experimental study along this direction.

References

[1] l'Huillier A, Lompre L A, Mainfray G and Manus C 1983 *Phys. Rev. A* **27** 2503
[2] Fittinghoff D N, Bolton P R, Chang B and Kulander K C 1992 *Phys. Rev. Lett.* **69** 2642
[3] Walker B, Sheehy B, Dimauro L F, Agostini P, Schafer K J and Kulander K C 1994 *Phys. Rev. Lett.* **73** 1227
[4] Becker W, Liu X J, Ho P J and Eberly J H 2012 *Rev. Mod. Phys.* **84** 1011
[5] Ma X M, Zhou Y M, Chen Y B, Li M, Li Y, Zhang Q B and Lu P X 2019 *Opt. Express* **27** 1825
[6] Huang C, Zhong M M and Wu Z M 2018 *Opt. Express* **26** 26045
[7] Eckart S, Richter M, Kunitski M *et al.* 2016 *Phys. Rev. Lett.* **117** 133202
[8] Milošević D B, Becker W and Kopold R 2000 *Phys. Rev. A* **61** 063403
[9] Hasović E, Becker W and Milošević D B 2016 *Opt. Express* **24** 6413
[10] Milošević D B and Becker W 2016 *Phys. Rev. A* **93** 063418
[11] Yuan K J, Chelkowski S and Bandrauk A D 2016 *Phys. Rev. A* **93** 053425
[12] Lin K, Jia X Y, Yu Z Q *et al.* 2017 *Phys. Rev. Lett.* **119** 203202
[13] Xu T T, Zhu Q Y, Chen J H, Ben S, Zhang J and Liu X S 2018 *Opt. Express* **26** 1645
[14] Weber Th, Giessen H, Weckenbrock M *et al.* 2000 *Nature* **405** 658
[15] Xu T T, Ben S, Wang T, Zhang J, Guo J and Liu X S 2015 *Phys. Rev. A* **92** 033405
[16] Weckenbrock M, Zeidler D, Staudte A *et al.* 2004 *Phys. Rev. Lett.* **92** 213002
[17] Xu T T, Chen J H, Pan X F, Zhang H D, Ben S and Liu X S 2018 *Chin. Phys. B* **27** 093201
[18] Liu X, Rottke H, Eremina E *et al.* 2004 *Phys. Rev. Lett.* **93** 263001
[19] Liu Y Q, Fu L B, Ye D F, Liu J, Li M, Wu C Y, Gong Q H, Moshammer R and Ullrich J 2014 *Phys. Rev. Lett.* **112** 013003
[20] Chen J and Nam C H 2002 *Phys. Rev. A* **66** 053415
[21] Song K L, Yu W W, Ben S, Xu T T, Zhang H D, Guo P Y and Guo J 2017 *Chin. Phys. B* **26** 023204
[22] Parker J S, Doherty B J S, Taylor K T, Schultz K D, Blaga C I and DiMauro L F 2006 *Phys. Rev. Lett.* **96** 133001
[23] Ma X M, Zhou Y M and Lu P X 2016 *Phys. Rev. A* **93** 013425
[24] Xu T T, Ben S, Zhang J and Liu X S 2017 *J. Phys. B: At. Mol. Opt. Phys.* **50** 105401
[25] Feuerstein B, Moshammer R, Fischer D *et al.* 2001 *Phys. Rev. Lett.* **87** 043003
[26] Bergues B, Kübel M, Johnson N G *et al.* 2012 *Nat. Commun.* **3** 813
[27] Huang C, Zhou Y M, Zhang Q B and Lu P X 2013 *Opt. Express* **21** 11382
[28] Ben S, Wang T, Xu T T, Guo J and Liu X S 2016 *Opt. Express* **24** 7525
[29] Zhang L, Xie X H, Roither S *et al.* 2014 *Phys. Rev. Lett.* **112** 193002
[30] Yuan Z Q, Ye D F, Xia Q Z, Liu J and Fu L B 2015 *Phys. Rev. A* **91** 063417
[31] Mancuso C A, Hickstein D D, Dorney K M *et al.* 2016 *Phys. Rev. A* **93** 053406
[32] Gazibegović-Busuladžić A, Becker W and Milošević D B 2018 *Opt. Express* **26** 12684
[33] Chaloupka J L and Hickstein D D 2016 *Phys. Rev. Lett.* **116** 143005
[34] Mancuso C A, Dorney K M, Hickstein D D *et al.* 2016 *Phys. Rev. Lett.* **117** 133201
[35] Ben S, Guo P Y, Pan X F, Xu T T, Song K L and Liu X S 2018 *Chem. Phys. Lett.* **706** 62
[36] Hu S X 2013 *Phys. Rev. Lett.* **111** 123003
[37] Liu A H and Thumm U 2014 *Phys. Rev. A* **89** 063423
[38] Zhou Y M, Liao Q and Lu P X 2010 *Phys. Rev. A* **82** 053402
[39] Ye D F, Liu X and Liu J 2008 *Phys. Rev. Lett.* **101** 233003
[40] Fu L B, Xin G G, Ye D F and Liu J 2012 *Phys. Rev. Lett.* **108** 103601
[41] Zhou Y M, Huang C, Tong A H, Liao Q and Lu P X 2011 *Opt. Express* **19** 2301
[42] Wang X and Eberly J H 2009 *Phys. Rev. Lett.* **103** 103007
[43] Ammosov M V, Delone N B and Krainov V P 1986 *Zh. Eksp. Teor. Fiz.* **91** 2008
[44] Delone N B and Krainov V P 1991 *J. Opt. Soc. Am. B* **8** 1207
[45] Leopold J G and Percival I C 1979 *J. Phys. B* **12** 709
[46] Li N, Zhou Y M, Ma X M, Li M, Huang C and Lu P X 2017 *J. Chem. Phys.* **147** 174302
[47] Luo S Q, Ma X M, Xie H, Li M, Zhou Y M, Cao W and Lu P X 2018 *Opt. Express* **26** 13666
[48] Corkum P B, Burnett N H and Brunel F 1989 *Phys. Rev. Lett.* **62** 1259
[49] Kopold R, Milošević D B and Becker W 2000 *Phys. Rev. Lett.* **84** 3831
[50] Mauger F, Chandre C and Uzer T 2010 *Phys. Rev. Lett.* **105** 083002
[51] Wang X, Tian J and Eberly J H 2013 *Phys. Rev. Lett.* **110** 073001